The 12th International Symposium on Visual Computing (ISVC)
December 12-14, 2016 Las Vegas, Nevada, USA.

Automated Rebar Detection for Ground-Penetrating Radar

Spencer Gibb and Hung Manh La(✉)

University of Nevada, Reno, USA
hla@unr.edu

Abstract. Automated rebar detection in images from ground-penetrating radar (GPR) is a challenging problem and difficult to perform in real-time as a result of relatively low contrast images and the size of the images. This paper presents a rebar localization algorithm, which can accurately locate the pixel locations of rebar within a GPR scan image. The proposed algorithm uses image classification and statistical methods to locate hyperbola signatures within the image. The proposed approach takes advantage of adaptive histogram equalization to increase the visual signature of rebar within the image despite low contrast. A Naive Bayes classifier is used to approximately locate rebar within the image with histogram of oriented gradients feature vectors. In addition, a histogram based method is applied to more precisely locate individual rebar in the image, and then the proposed methods are validated using existing GPR data and data collected during the course of the research for this paper.

1 Introduction

GPR has been increasingly used in applications for structural surveys since the 1980s [1]. Uses for GPR include bridge integrety inspection [1,2], metro tunnel inspection [3], beam and pillar structural inspection, as well as many others. GPR provides a visual representation of metallic objects underneath concrete surfaces, which are indicated by their hyperbolic signatures in the scan image. Prior to recent research in automated object detection using GPR, object location was done manually or using commercial software [4]. Manually locating objects in a scan can be extremely time consuming considering scans can contain hundreds of rebar depending on the size of the bridge being inspected and commercial software costs thousands of dollars in some cases; when combined with the cost of GPR itself, this can easily prevent users from successfully using the technology.

With the end goal of moving toward a fully automated solution for bridge inspection, the primary concerns with modern methods are detection accuracy and the ability to perform detection in real-time. While research is still continuing in this field, recent methods utilize support vector machines, gradient descent, and various computationally intense methods for detecting rebar [5–9]. The accuracy of some of these methods has been high, but they are typically tested on ideal cases where scan data is not representative of aged structures,

G. Bebis et al. (Eds.): ISVC 2016, Part I, LNCS 10072, pp. 815–824, 2016.
DOI: 10.1007/978-3-319-50835-1_73

or simulated data, and they often have too high of a run time to be performed on site [10–12].

This paper presents a novel method for automated rebar localization that can be performed in real-time, with scans from long bridges being run in a short amount of time. The proposed method in this paper utilizes adaptive histogram equalization to eliminate difficulties caused by low contrast images with regard to the hyperbola signatures being too faint to detect. A Naive Bayes classifier, which has been shown to be sufficient for simple classification tasks [13], is used to approximately locate rebar within the image, and then a simple method developed for this paper is employed, called histogram localization. This method combines histogram maxima detection with a local search for maximum pixel intensity that can more precisely locate the vertex of the hyperbolic signature for each rebar in the image.

The remainder of the paper is organized as follows. Section 2 provides a description of the need for and application of adaptive histogram equalization. Section 3 describes the features used for the image classifier. Section 4 describes the training of the Naive Bayes classifier. Section 5 outlines the central concepts of the Naive Bayes classifier used. Section 6 details the methods used to more precisely localize the rebar within the scan image. Experimental results are provided in Sect. 7. Lastly, a conclusion is provided in Sect. 8.

2 Adaptive Histogram Equalization for Contrast Stretching

Due to the typically low-contrast nature of B-scan images obtained via GPR scans, it is necessary to stretch the contrast of these images prior to feature extraction, training, and classification [14]. Contrast stretching helps strengthen the accuracy of the image classifier and makes it easier for humans to verify the work of the classifier, since it is often difficult or impossible to locate objects in low contrast images. Because standard histogram equalization leads to artifacts in the images, contrast stretching is accomplished in this paper through Contrast Limited Adaptive Histogram Equalization (CLAHE) [15]. Peaks in a histogram are typically attributed to uniform regions in an image, and through the equalization process the intensity values within the image that correspond to the peaks are spread out across a wider range of intensity values. Although spreading peaks in this way is the primary use for histogram equalization, as it applies contrast stretching and compression, issues can arise when uniform regions of an image contain noise. The noise in uniform regions is then spread across the image as equalization is applied, which can lead to artifacts as the noise is overamplified throughout the image. The CLAHE algorithm presents a solution to this problem that allows adaptive histogram equalization to be performed without propagating noise across the image.

Given an image I, which is M by N pixels, histogram equalization is applied across nonoverlapping regions of the image sized $M/8$ by $N/8$ pixels, in the same manner as adaptive histogram equalization. However, the difference between the

CLAHE method and standard adaptive histogram equalization is that a clip limit is set, which prevents noise being overamplified in homogeneous regions of the image and causing artifacts. The clip limit is used to determine how much of the histogram's peak to remove prior to calculating the cumulative distribution function that is used in that region. The part of the histogram peak that is clipped can be redistributed across the bins of the histogram so that it is still present and does not incorrectly skew the cumulative distribution function of the image. When histogram equalization is applied to a GPR image with low contrast it typically leads to areas of the image being too bright or too dark. On the other hand, when CLAHE is applied, the bright areas and dark areas are less prevalent, which makes it easier to classify regions of the image because the image has more defined features.

3 Histogram of Oriented Gradients as Hyperbola Features

Histogram of oriented gradients (HOG) was originally described by Dalal and Triggs in 2005 as a feature descriptor used for object detection [16]. This method uses gradient orientation across an image that is split into uniform cells. HOG features are invariant to geometric transformations and illumination and can be quickly computed. As a result, HOG features have been widely used for object detection in computer vision problems since 2005 [17,18]. The steps for computing HOG features used in this paper are as follows.

Given a grayscale image I, the image can be globally normalized to make the feature selection process more invariant to illumination. Then first order gradients of the normalized image must be computed as

$$\nabla I_N = \begin{bmatrix} g_x \\ g_y \end{bmatrix} \tag{1}$$

where g_x and g_y are the normalized image gradients in the x and y direction respectively and I_N is the normalized image. The magnitude of the normalized image is given by

$$magnitude(I_N) = \sqrt{g_x^2 + g_y^2} \tag{2}$$

and the orientation of the normalized image is given by

$$\theta = atan2(g_y, g_x) * (180/\pi) + 90. \tag{3}$$

The image is then segmented into cells. In this paper, it was empirically determined that 5 by 5 pixel cells yielded the best results throughout the training and classification processes. The training and testing image size used in this paper is 50 by 15 pixels, which means that each training and testing image is made up of 30 cells. For each of the cells, a histogram of gradient orientations is accumulated. Finally, to increase the invariance of this method to illumination, block normalization is applied. Blocks consist of several cells; 3 cell by 3 cell

blocks were used in this paper. The cells are normalized within respective blocks yielding final image descriptors. The features vectors used in the training and classification methods for this paper contain 240 elements, as each image is 10 by 3 cells and 8 bins were used for the accumulation of histograms of oriented gradients.

4 Training

In order to train the Naive Bayes classifier used in this paper, HOG features are extracted from a set of manually selected training images, comprised of two classes: images containing hyperbolas that would indicate the presence of rebar in a GPR scan, and images that do not contain hyperbolas. Each of the selected images is manually assigned a class label for the purpose of training the classifier. The classifier in the next section uses the information from the determined HOG feature vectors for training images as a basis for a priori knowledge about each class. Infomation on the number of training images and the class they belong to can be seen in Table 1. In addition, examples of training images can be seen in Fig. 1.

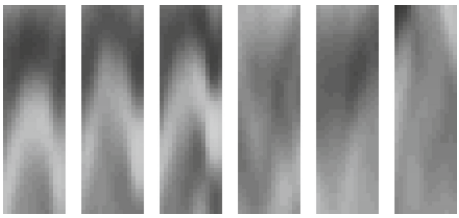

Fig. 1. (a)–(c) Positive samples used in the training process that contain clear hyperbolas indicating the presence of rebar; (d)–(f) Negative samples used in the training process that do not contain a hyperbola. Each of these 6 samples is 50 by 15 pixels.

Table 1. Training data set

Class	Class name	Number of images
1	Hyperbolas	304
2	Not Hyperbolas	1800

5 Naive Bayes Classification

A Naive Bayes classifier is used in this paper that classifies new GPR images based on their computed HOG feature vectors, as well as the feature vectors from the training images. More advanced methods are not necessary since the classifier is not solely responsible for the location of rebar in a GPR scan. This classifier was chosen for its simplicity and speed.

Given a vector of HOG features $x = (x_1, ..., x_n)$, where n is the number of features in the vector, Bayes' theorem states that the probability of a class given

a sample is the product of the a priori probility for that class and the probability of the sample given the class. The Bayes model can be written as

$$p(C_k|x) = \frac{1}{Z} p(C_k) \prod_{i=1}^{n} p(x_i|C_k) \tag{4}$$

where Z is a constant scaling factor that depends on the contents of the feature vector and C_k is class k. Z will change depending on the implementation of the Naive Bayes classifier.

The model from Eq. (4) can be used as a classifier to assign class labels to test samples as follows

$$\hat{y} = \underset{k \in \{1,\ldots,K\}}{\arg\max}\ p(C_k) \prod_{i=1}^{n} p(x_i|C_k) \tag{5}$$

where $\hat{y}$ is the assigned class label given a sample, which is chosen based on the maximum probability of a class given the sample. This method, the maximum a posteriori probability (MAP) estimate, classifies solely based on the posteriori probability determined by the Naive Bayes classifier for each class.

Prior to using this Naive Bayes classifier, a search area is determined in the test image. The search area is located based on a primary trait of all GPR scan images; they all contain a significant dark region in the image where the ground surface is. No searching should be done higher in the image than the ground surface. Once the ground surface is located through finding large occurrences of dark horizontal intensity values, the search window is limited again by performing edge detection on the area of the image below the ground plane. The end of the search area is given by taking the average y pixel location of each edge pixel and searching up to that average location. This works because the edge information shows where the general rebar location is along the y axis.

Searching and classfication is performed on a sliding window starting from just below the ground plane to the average y location of edges determined previously. The distance of this classification search can be changed in cases where bridge decks may contain rebar that is sporadically located along the y axis of the image; however, significantly expanding the search window limits the real-time capabilities of any method including those outlined in this paper. In addition, to limit the time it takes to apply the sliding window, odd numbered y coordinates are skipped since they do not affect the accuracy of this method and only increase its run time. At each sliding window location within the search area, if the classifier assigns a hyperbola class label to the test image, that point is saved for further processing to more exactly localize hyperbolas within the image.

In the previous sections, an image is first contrast stretched using adaptive histogram equalization. Then the search area within the image is determined using edge detection and the location of the ground plane. Next, training is performed on previously selected images. Then classification is performed on a sliding window, using HOG features, accross the search window within the image.

6 Final Localization of Rebar

Given a set of points in the original image, P_{IN}, indicating where a hyperbola was detected and classified by the Naive Bayes classifier, it is necessary to more accurately localize the hyperbola. Typical methods for hyperbola localization and fitting include use of the Hough transform or RANSAC [6,7]. However, both of these methods are typically time consuming and therefore not ideal for real-time applications such as that of online automated rebar detection. The methods used in this paper provide a real-time solution, we refer to as histogram localization, that is of linear time-complexity, since it just moves through a list of pixels in each step that only increases in size as the size of the image and number of pixels increases. This method also allows for accurate rebar localization.

The points in the image are used to accumulate a histogram of their x coordinates. From the accumulated histogram, local maxima are preserved while non-maxima are suppressed in order to yield a set of vertical lines indicating the locations of the most positive matches in a local area. In this paper, a 13 pixel wide area was used to choose local maxima, which were allowed during this step since they will be eliminated as they converge to the same point in following steps.

After histogram localization is performed, the pixels on each vertical line are compared against each other to find the location of the maximum intensity value. The pixel with the maximum intensity value is significant because the nature of GPR means that objects in the image with high intensity values are typically metallic and rebar is the object that is being located. Once the highest intensity pixels along each vertical line are located, another search is performed for local maxima within a 5 pixel by 5 pixel region surrounding each of the high intensity pixels.

A final maxima search allows for any location that may be too low on the rebar or that may be off center to be correctly localized, which also accounts for multiple local maxima in the previous step since these maxima typically converge to the same point. For multiple remaining maxima, the maxima closest to the top of the image can be chosen. This should be performed on a small window to ensure that correct positives are not ignored. A summary of the previously described algorithm can be seen in Algorithm 1.

7 Experimental Results

The methods proposed in this paper have been validated on scans from three bridges that were collected prior to the research done for this paper and provided by Geophysical Survey Systems, Inc., as well as scans from a bridge that were collected during the course of this research. All processing was done on a 5-year-old system running an i5 2500k processor. Rebar detection results can be seen in Table 2. Included in the results is the average run time for images of each bridge, accuracy, precision, and the number of rebar that were present in the GPR images of each bridge, as well as the location of each bridge. Examples of rebar localization (red squares) can be seen in Fig. 2.

Algorithm 1. Precise Hyperbola Localization

Input: $P_{IN} = \{P_1, P_2, ..., P_n\} | P_n = (x_n, y_n)$
s = starting search location
e = ending search location
Output: $P_{OUT} = \{P_1, P_2, ..., P_3\}$

```
x_histogram[Image width] for x ← P_IN[0][0] to P_IN[n][0] do
    x_histogram[x] += 1
for i ← 0 to x_histogram length do
    if x_histogram[i] > 0 then
        maxima ← true
        Maxima_list ← [ ]
        for j ← i − 7 to i + 6 do
            if j > −1 and j < x_histogramlength then
                if x_histogram[j] > x_histogram[i] then
                    maxima ← false
        if maxima == true then
            append maxima to Maxima_list
x_coords ← [ ]
y_coords ← [ ]
for i ← 0 to Maxima_list length do
    x ← −1
    y ← −1
    for j ← search_start to search_end do
        if Image[j, Maxima_list[i]] > x then
            x ← Image[j, Maxima_list[i]]
            y ← j
    append x to x_coords
    append y to y_coords
P_OUT ← [ ]
for i ← 0 to x_coords length do
    x ← x_coords[i]
    y ← y_coords[i]
    intensity ← Image[x, y]
    final_x ← −1
    final_y ← −1
    for j ← y − 3 to y + 2 do
        for k ← x − 3 to x + 2 do
            if Image[j, k] > intensity then
                intensity ← Image[j, k]
                final_x ← k
                final_y ← j
    append (final_x, final_y) to P_OUT
```

Table 2. Automated rebar detection results.

Bridge name	Location	Number of GPR images	Total rebar in images	Accuracy	Precision	Run time/image
East Helena Bridge	Helena, MT	14	1055	99.15%	98.22%	32.40 s
Kendall Pond Road Bridge	Derry, NH	12	2284	91.46%	97.79%	32.91 s
Ramp D	Lewiston, ME	14	3699	92.89%	93.787%	55.46 s
Pleasant Valley Bridge	Reno, NV	20	13206	96.67%	99.59%	118.32 s

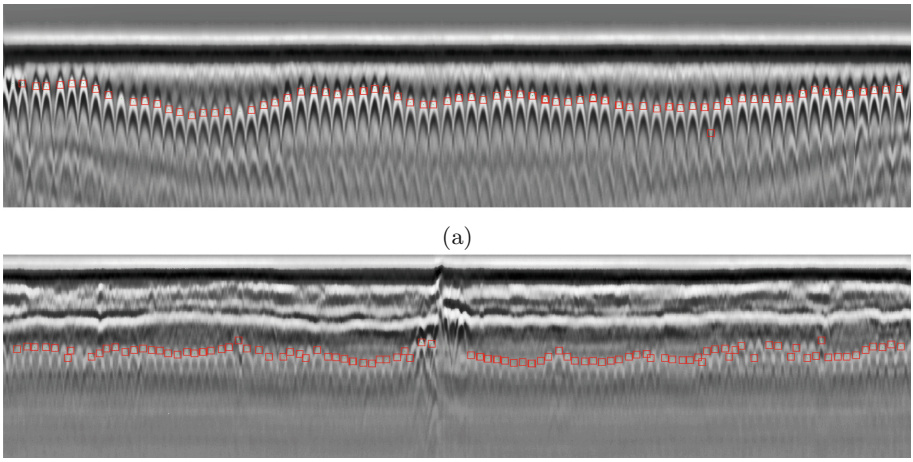

(a)

(b)

Fig. 2. Rebar localization results (red squares): (a) GPR image from East Helena Bridge, Helena, MT; (b) GPR image from Kendall Pond Road Bridge, Derry, NH. (Color figure online)

The results show that this method performs well on the data from the four bridges used in this paper. The accuracy of the proposed method decreases slightly in cases where adaptive histogram equalization did not affect how clear the hyperbolas are. This is the case with the photos of the Kendall Pond Road Bridge in New Hampshire, which had feint hyperbola. In addition, the classifier performs better in cases where hyperbola are clearly visually separable, as opposed to in cases where they are cluttered and appear to overlap. In cases of overlap, some rebar will not be detected. Overall, the precision of the proposed method remains high, indicating that rebar are not found in areas where none exist.

Finally, with respect to run time of the proposed method, it performs well in all cases. Increased run time is proportional to the length of the bridge. A longer bridge usually contains more rebar and therefore requires more processing.

However, all of the run times listed in this paper are short enough that they can be run as part of a fully autonomous robotic system, in real-time [19,20].

8 Conclusion and Future Work

This paper proposed a real-time automated rebar detection method, which combines adaptive histogram equalization, HOG features, and a Naive Bayes classifier. The proposed method works in real-time to accurately detect rebar in GPR scan images. Moreover, it has been validated through tests run on four sets of real bridge data. Future work in this area of research will include the use of this software in a fully autonomous robotic bridge inspection system. In addition, increased invariance to varying bridge conditions and further real-time capability will be researched. Fusion of GPR data with other nondestructive evaluation (NDE) sensors will be also studied for enhancing the condition assessment of the bridge deck [21,22].

Acknowledgment. The authors would like to thank the University of Nevada, Reno and the National Science Foundation (NSF) for their financial support to conduct this research: NSF support under grant: NSF-IIP # 1639092.

References

1. Simi, A., Manacorda, G., Benedetto, A.: Bridge deck survey with high resolution ground penetrating radar. In: 2012 14th International Conference on Ground Penetrating Radar (GPR), pp. 489–495 (2012)
2. Krause, V., Abdel-Qader, I., Abudayyeh, O.: Detection and classification of small perturbations in GPR scans of reinforced concrete bridge decks. In: 2012 IEEE International Conference on Electro/Information Technology (EIT), pp. 1–4 (2012)
3. Hai-zhong, Y., Yu-feng, O., Hong, C.: Application of ground penetrating radar to inspect the metro tunnel. In: 2012 14th International Conference on Ground Penetrating Radar (GPR), pp. 759–763 (2012)
4. Marecos, V., Fontul, S., Antunes, M.L., Solla, M.: Assessment of a concrete prestressed runway pavement with ground penetrating radar. In: 2015 8th International Workshop on Advanced Ground Penetrating Radar (IWAGPR), pp. 1–4 (2015)
5. Shaw, M., Millard, S., Molyneaux, T., Taylor, M., Bungey, J.: Location of steel reinforcement in concrete using ground penetrating radar and neural networks. NDT E Int. **38**, 203–212 (2005). Structural Faults and Repair
6. Kaur, P., Dana, K.J., Romero, F.A., Gucunski, N.: Automated GPR rebar analysis for robotic bridge deck evaluation. IEEE Trans. Cybern. **46**, 2265–2276 (2016)
7. Al-Nuaimy, W., Huang, Y., Nakhkash, M., Fang, M., Nguyen, V., Eriksen, A.: Automatic detection of buried utilities and solid objects with GPR using neural networks and pattern recognition. J. Appl. Geophys. **43**, 157–165 (2000)
8. La, H.M., Lim, R.S., Basily, B.B., Gucunski, N., Yi, J., Maher, A., Romero, F.A., Parvardeh, H.: Mechatronic systems design for an autonomous robotic system for high-efficiency bridge deck inspection and evaluation. IEEE/ASME Trans. Mechatron. **18**, 1655–1664 (2013)

9. La, H.M., Gucunski, N., Kee, S.H., Yi, J., Senlet, T., Nguyen, L.: Autonomous robotic system for bridge deck data collection and analysis. In: 2014 IEEE/RSJ International Conference on Intelligent Robots and Systems, pp. 1950–1955 (2014)
10. Xianqi-He, Z.-Z., Guangyin-Lu, Q.-L.: Bridge management with GPR. In: 2009 International Conference on Information Management, Innovation Management and Industrial Engineering, vol. 3, pp. 325–328 (2009)
11. Pasolli, E., Melgani, F., Donelli, M.: Automatic analysis of GPR images: a pattern-recognition approach. IEEE Trans. Geosci. Remote Sens. **47**, 2206–2217 (2009)
12. Zhao, Y., Chen, J., Ge, S.: Maxwell curl equation datuming for GPR test of tunnel grouting based on kirchhoff integral solution. In: 2011 6th International Workshop on Advanced Ground Penetrating Radar (IWAGPR), pp. 1–6 (2011)
13. Shi, H., Liu, Y.: Naïve Bayes vs. support vector machine: resilience to missing data. In: Deng, H., Miao, D., Lei, J., Wang, F.L. (eds.) AICI 2011. LNCS (LNAI), vol. 7003, pp. 680–687. Springer, Heidelberg (2011). doi:10.1007/978-3-642-23887-1_86
14. Wang, Z.W., Zhou, M., Slabaugh, G.G., Zhai, J., Fang, T.: Automatic detection of bridge deck condition from ground penetrating radar images. IEEE Trans. Autom. Sci. Eng. **8**, 633–640 (2011)
15. Pizer, S.M., Amburn, E.P., Austin, J.D., Cromartie, R., Geselowitz, A., Greer, T., Romeny, B.T.H., Zimmerman, J.B.: Adaptive histogram equalization and its variations. Comput. Vis. Graph. Image Process. **39**, 355–368 (1987)
16. Dalal, N., Triggs, B.: Histograms of oriented gradients for human detection. In: 2005 IEEE Computer Society Conference on Computer Vision and Pattern Recognition (CVPR 2005), vol. 1, pp. 886–893 (2005)
17. Pang, Y., Zhang, K., Yuan, Y., Wang, K.: Distributed object detection with linear SVMs. IEEE Trans. Cybern. **44**, 2122–2133 (2014)
18. Nigam, S., Khare, M., Srivastava, R.K., Khare, A.: An effective local feature descriptor for object detection in real scenes. In: 2013 IEEE Conference on Information Communication Technologies (ICT), pp. 244–248 (2013)
19. Lim, R.S., La, H.M., Shan, Z., Sheng, W.: Developing a crack inspection robot for bridge maintenance. In: 2011 IEEE International Conference on Robotics and Automation (ICRA), pp. 6288–6293 (2011)
20. Lim, R.S., La, H.M., Sheng, W.: A robotic crack inspection and mapping system for bridge deck maintenance. IEEE Trans. Autom. Sci. Eng. **11**, 367–378 (2014)
21. La, H.M., Gucunski, N., Kee, S.H., Nguyen, L.V.: Data analysis and visualization for the bridge deck inspection and evaluation robotic system. Visual. Eng. **3**, 6 (2015)
22. La, H.M., Gucunski, N., Lee, S.H., Nguyen, L.V.: Visual and acoustic data analysis for the bridge deck inspection robotic system. In: The 31st International Symposium on Automation and Robotics in Construction and Mining (ISARC), pp. 50–57 (2014)